iScience

CellPress
OPEN ACCESS

Article

S100A9 aggravates early brain injury after subarachnoid hemorrhage via inducing neuroinflammation and inflammasome activation

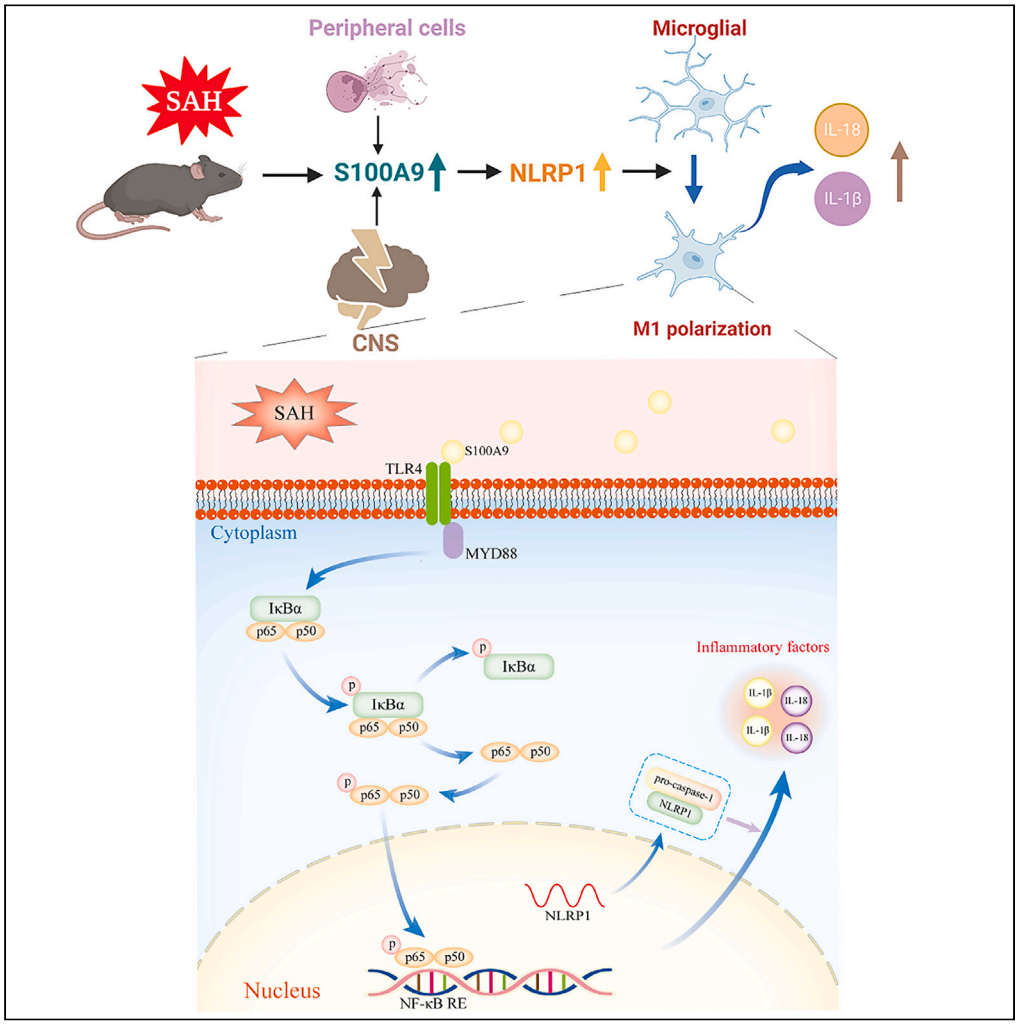

Guijun Wang, Kesheng Huang, Qi Tian, ..., Zhui Yu, Zhan Zhang, Mingchang Li

yuzhui@whu.edu.cn (Z.Y.)
doctorzhang2003@163.com (Z.Z.)
mingcli@whu.edu.cn (M.L.)

Highlights

The relationship between S100A9 protein and subarachnoid hemorrhage was revealed

S100A9 protein aggravates neuroinflammation after subarachnoid hemorrhage

S100A9 protein affects the prognosis of patients with subarachnoid hemorrhage

Wang et al., iScience 27, 109165
March 15, 2024 © 2024 The Author(s).
https://doi.org/10.1016/j.isci.2024.109165

iScience

CellPress
OPEN ACCESS

Article

S100A9 aggravates early brain injury after subarachnoid hemorrhage via inducing neuroinflammation and inflammasome activation

Guijun Wang,[1,4] Kesheng Huang,[1,2,4] Qi Tian,[1,4] Yujia Guo,[1] Chengli Liu,[1] Zhijie Li,[1] Zhui Yu,[2,*] Zhan Zhang,[3,*] and Mingchang Li[1,5,*]

SUMMARY

Subarachnoid hemorrhage (SAH) is a stroke subtype with high mortality, and its severity is closely related to the short-term prognosis of SAH patients. S100 calcium-binding protein A9 (S100A9) has been shown to be associated with some neurological diseases. In this study, the concentration of S100A9 in clinical cerebrospinal fluid samples was detected by enzyme-linked immunosorbent assay (ELISA), and the relationship between S100A9 and the prognosis of patients was explored. In addition, WT mice and S100A9 knockout mice were used to establish an *in vivo* SAH model. Neurological scores, brain water content, and histopathological staining were performed after a specified time. A co-culture model of BV2 and HT22 cells was treated with heme chloride to establish an *in vitro* SAH model. Our study confirmed that the expression of S100A9 protein in the CSF of SAH patients is increased, and it is related to the short-term prognosis of SAH patients. S100A9 protein is highly expressed in microglia in the central nervous system. S100A9 gene knockout significantly improved neurological function scores and reduced neuronal apoptosis. S100A9 protein can activate TLR4 receptor, promote nuclear transcription of NF-κB, increase the activation of inflammatory body, and ultimately aggravate nerve injury.

INTRODUCTION

Subarachnoid hemorrhage (SAH) is a type of stroke that accounts for 3–5% of all stroke cases and is characterized by a high mortality and poor prognosis.[1] Approximately 35 percent of patients die within 48 h after SAH.[2] The majority of SAH cases are caused by the rupture of the intracranial aneurysm, and the occurrence of intracranial aneurysms may be related to genetic factors.[3] Based on previous studies, early brain injury (EBI), which refers to the process of pathological changes in brain tissue, is caused within 72 h after SAH, and a significant proportion of survivors develop long-term neurological deficits.[4,5] There are many key factors leading to poor prognosis after SAH, with EBI being the most studied in recent years.[6] After SAH, the blood-brain barrier (BBB) is destroyed, and neuroinflammation and oxidative stress occurred,[7] which are the main mechanisms leading to EBI. Recently, neurorestorative therapeutic explorations have been conducted to try improving those damaged or lost functions due to SAH or stroke and brain injury.

Neuroinflammation occurs in the early stages of SAH and has been shown to lead to neuronal apoptosis.[8] In the past, cerebral artery spasm was considered the main cause of secondary brain injury,[9] but in recent years, the activation of neuroinflammation has gradually been recognized as one of the mechanisms of secondary brain injury.[10] The pathological processes in brain tissues after SAH are complex, and the underlying mechanisms have been extensively studied, among which the TLR4 (toll-like receptor 4) pathway is one of the most widely studied pathways.[11–13] The inflammatory response of the body usually takes the form of a pathogen-associated molecular pattern (PAMP) or damage-associated molecular pattern (DAMP), with pattern recognition receptors (PRRs) sensing these patterns and initiating immune responses. One of the most characterized PRR families is the TLR family, and TLR4 has recently come into focus as a key player in neuroinflammation.[14–16]

Alarmins, also known as DAMPs, are released after macrophage activation and play critical roles in innate immunity. The most prominent members of the DAMP family are heat-shock proteins (HSPs), high-mobility group protein B1 (HMGB1), calcium-binding protein S100A9 (also known as myeloid-related protein 14 [MRP-14]), and its binding partner S100A8 (also known as MRP-8).[17] Neutrophils and monocytes are the most important sources of S100A8 and S100A9, which form stable heterodimers or homodimers, respectively. Both S100A8 and S100A9 have a helix-loop-helix motif with charged amino acid residues, which leads to strong binding to divalent ions. After binding, their conformations changes, and these proteins carryout their respective functions.[18] Extracellular S100A9 interacts with TLR4 and receptor for advanced

[1]Department of Neurosurgery, Renmin Hospital of Wuhan University, Wuhan 430060, Hubei Province, China
[2]Department of Critical Care Medicine, Renmin Hospital of Wuhan University, Wuhan 430060, Hubei Province, China
[3]Department of Rehabilitation Medicine, Renmin Hospital of Wuhan University, Wuhan 430060, Hubei Province, China
[4]These authors contribute equally
[5]Lead contact
*Correspondence: yuzhui@whu.edu.cn (Z.Y.), doctorzhang2003@163.com (Z.Z.), mingcli@whu.edu.cn (M.L.)
https://doi.org/10.1016/j.isci.2024.109165

This is an open access article under the CC BY-NC-ND license (http://creativecommons.org/licenses/by-nc-nd/4.0/).

A

Groups	Mortality	Exclude
Experiment 1		
Sham	0%(0/12)	0
SAH(3h, 6h, 12h, 24h, 72h)	22.64%(12/53)	5
Experiment 2		
Sham	0%(0/18)	0
WT-SAH(24h)	26.67%(8/30)	4
KO-SAH(24h)	21.43%(6/28)	4
Experiment 3		
Sham	0%(0/18)	0
WT-SAH(72h)	25%(7/28)	3
KO-SAH(72h)	20.69%(6/29)	5
Experiment 4		
Sham	0%(0/12)	0
SAH+Vehicle	25%(5/20)	3
SAH+ rS100A9	33.33%(7/21)	2
SAH-KO	20%(4/20)	4
SAH-KO+ rS10A9	28.57%(6/21)	3
Experiment 5		
Sham	0%(0/3)	0
SAH+Vehicle	33.3%(2/6)	1
SAH+ PDTC	20%(1/5)	1
SAH+PDTC+rS100A9	28.5%(2/7)	2
Total		
Sham	0%(0/63)	0
SAH: WT-SAH, KO-SAH	24.6% (66/268): 25.88%(44/170), 22.45%(22/98)	37: 21, 16

B

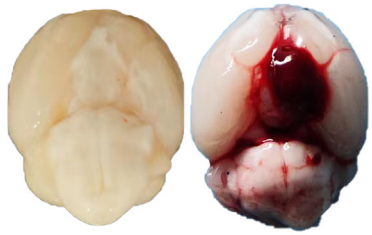

C

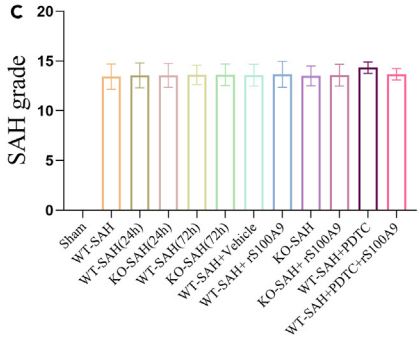

Figure 1. Animal groups, mortality, and SAH grading in mice

(A) Animal usage and mortality.

(B) Representative brain images from the SAH.

(C) SAH grading scores in each group. Data were represented as the mean ± SD.

glycation end products (RAGE), promoting cell activation and recruitment.[19] NLRP1 is an inflammatosome formation PRR that, like other family members (e.g., NLRP3[20]), also regulates cell death. The mechanism is that NLRP1 inflammatosomes are activated when stimulated by injury-associated molecular patterns, causing inflammation through the production of proinflammatory cytokines IL-18 and IL-1β.[21] S100A9 has been shown to be associated with many neurological diseases; therefore, this study aimed to investigate the relationship between S100A9 and neuroinflammation, and its mechanism after SAH.

RESULTS

SAH model mortality and grade score

A total of 63 mice were used in the sham-operated group, and 268 mice (170 WT and 98 KO mice) were used to establish SAH models. Finally, 37 mice were excluded (SAH grade score <8; Figure 1A). The overall mortality rate of the SAH modeling was 24.6% (66/268), and the mortality rates of WT and KO mice were 25.88% (44/170) and 22.45% (22/98), respectively. A representative schematic of the successful modeling of SAH is shown in Figure 1B. There was no significant difference in the SAH grade scores in all the SAH groups (Figure 1C, $p > 0.05$).

Temporal expression of S100A9 and TLR4

We used the GEO database analysis to identify differentially expressed genes between the ipsilateral cerebral hemispheres of the Sham and SAH groups (Figure 2A). Subsequently, we input the differentially expressed genes into the STRING database and plotted the genetic interaction network. This analysis showed that both S100A9 and TLR4 were upregulated in SAH (Figure 2B). Further, The expression of S100A9 and TLR4 protein *in vivo* was detected by western blotting (Figure 2C). The results showed that the expression of S100A9 and TLR4 began to increase significantly at 12 h, reached a peak at 24 h, and then decreased at 72 h (Figure 2C). Double immunofluorescence staining confirmed that S100A9 mainly colocalized with microglia (Figure 2D).

S100A9 knockout can improve neurological score after SAH and alleviate EBI

Neurological deficits were assessed using the modified Garcia score and the neurological score 24 h after SAH was analyzed. The neurobehavioral scores changed significantly after SAH compared with the sham group (Figures 3A and 3B), and these changes were reversed by S100A9 knockdown. Brain edema after SAH is closely associated with poor prognosis. The water content of the left and right hemispheres

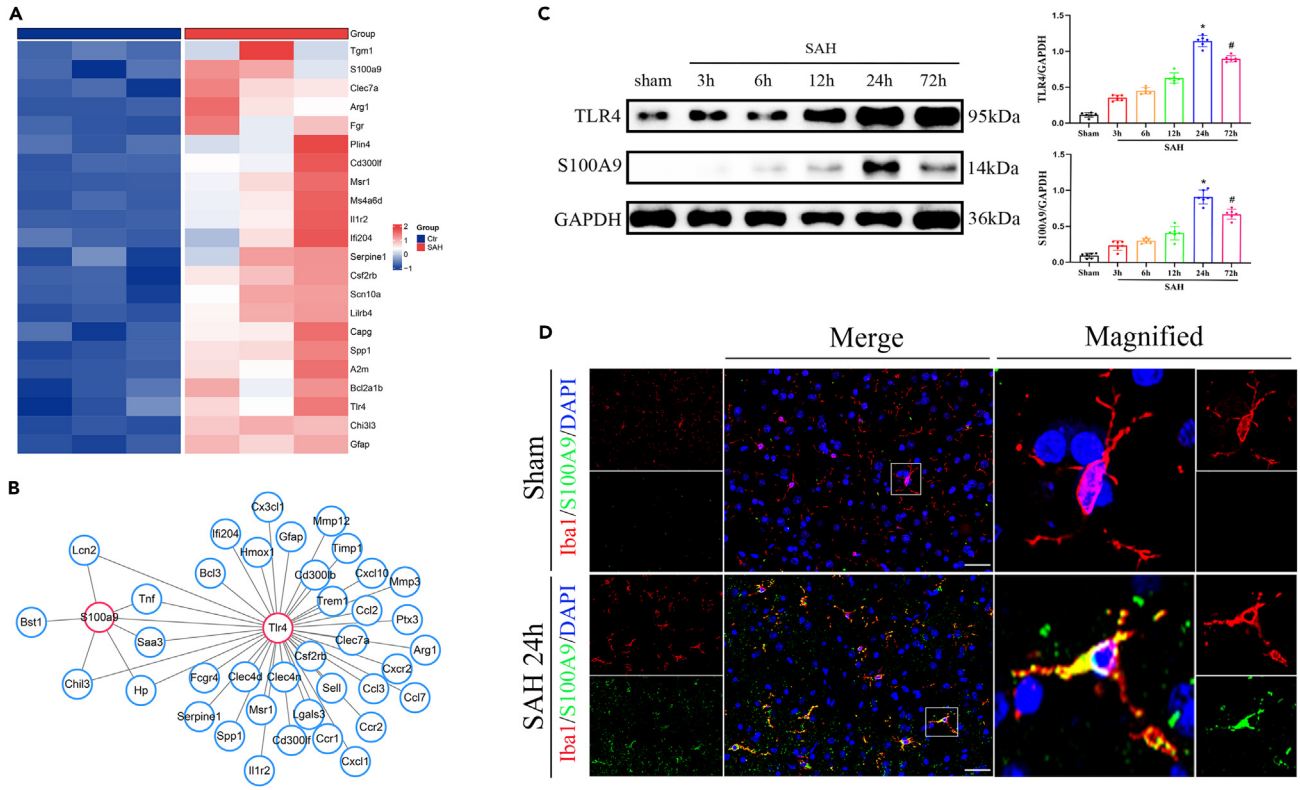

Figure 2. Expression and distribution of S100A9 and TLR4 after SAH in mice

(A) Heat maps revealed upregulated and downregulated genes in the sham and SAH groups.

(B) Network showing protein-protein interaction for the genes.

(C) Representative western blotting images and quantitative analyses of S100A9 and TLR4 expression after SAH. n = 6 per group. *p < 0.05 vs. Sham group; #p < 0.05 vs. SAH 24 h group.

(D) Representative images of double immunofluorescence staining for S100A9 in microglia at 24 h after SAH. n = 6 per group. Scale bar, 50 mm. Data were represented as the mean ± SD.

increased significantly 24 h after SAH. However, compared to WT mice, the brain water content of KO mice decreased after SAH (Figure 3C). We confirmed the absence of S100A9 expression in S100A9 knockout mice using western blotting (Figures 3D and 3E). H&E staining was used for pathological analysis of cortical and hippocampal neurons. The results showed that the number of neurons of the opposite sex increased in the cortex and hippocampus of the mice after SAH, and obvious edema appeared, which was ameliorated by S100A9 knockout (Figure 3F).

S100A9 knockout can improve neuronal apoptosis after SAH

We again used the modified Garcia and neurological scores to evaluate neurological function 72 h after SAH. The results were similar to the changes observed at 24 h (Figures 4A and 4B). TUNEL and Nissl staining were used to observe the degree of neuronal damage in the ipsilateral cortex and hippocampus after SAH. TUNEL staining showed that, compared with the sham group, the number of apoptotic neurons in the cortex of the mice increased after SAH, while S100A9 knockout reduced neuronal apoptosis. The results of Nissl staining showed that the number of neurons decreased mainly in the cortex, corneum area (CA) 1, CA3, and dentate gyrus (DG), and the neurons in these areas showed obvious atrophy 72 h after SAH (Figures 4E–4G). These changes were significantly ameliorated by S100A9 knockdown.

Paquinimod reduce neuronal apoptosis in an *in vitro* SAH model

We treated BV2 cells with hemin for 24 h. At the same time, the effects of hemin and paquinimod at different concentrations in BV2 cells were detected by CCK8 assay. The CCK8 assay results showed that cell viability decreased significantly after adding hemin, and the optimal concentration was 160 μmol/L hemin (cell viability 51.37 ± 3.13%; Figure 5A). In addition, the results also showed that 20 μmol/L paquinimod (resulting in cell viability 77.1 ± 2.60%) was the optimal treatment concentration after hemin induction of BV2 cells (Figure 5B).

BV2 and HT22 cells were co-cultured in a hemin-containing medium to explore the effect of S100A9 on the apoptosis of HT22 cells *in vitro* (Figure 5C). Neuronal apoptosis was significantly increased after heme addition compared with that in the control. Paquinimod administration reversed hemin-induced apoptosis (Figures 5D and 5E). Flow cytometry confirmed that paquinimod reversed hemin-induced apoptosis (Figures 5F and 5G).

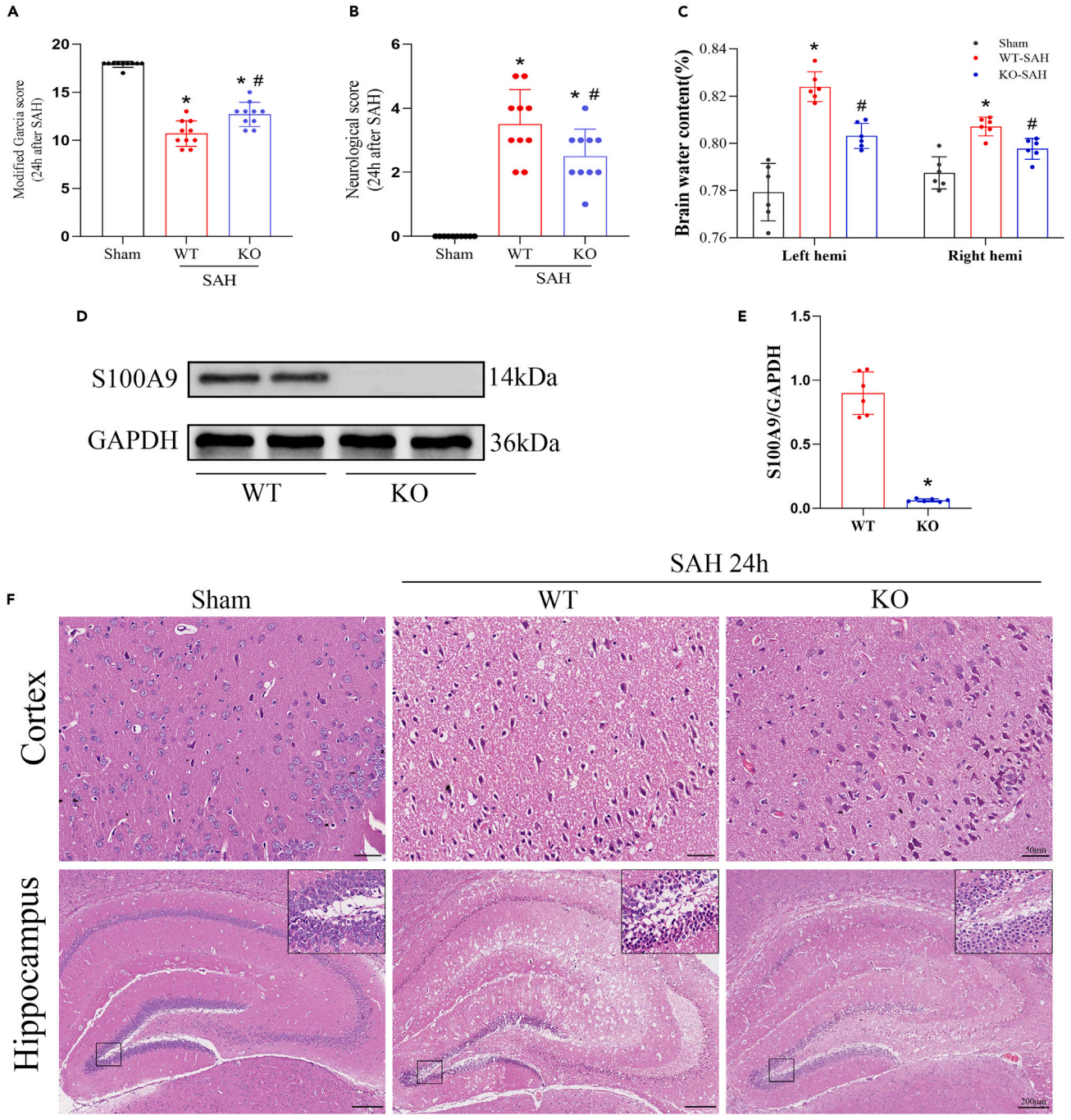

Figure 3. S100A9 knockout can improve neurological deficit, brain edema, and reduce the damage of cortex and hippocampus after SAH 24 h

(A and B) The modified Garcia and neurological score of each group. n = 10 per group. *$p < 0.05$ vs. Sham group; $^{\#}p < 0.05$ vs. WT-SAH group.

(C) Quantification of brain water content. n = 6 per group. *$p < 0.05$ vs. Sham group; $^{\#}p < 0.05$ vs. WT-SAH group.

(D and E) Representative picture and quantitative analysis of western blotting from S100A9 knockout mice. n = 6 per group. *$p < 0.05$ vs. WT group.

(F) Representative H&E staining images of brain slides. n = 6 per group. Scale bar, 50/200 μm. Data were represented as the mean ± SD.

S100A9 aggravates nerve injury by inducing neuroinflammation and activating NLRP1 inflammasome

To further explore the relationship between S100A9 and neuroinflammation, we introduced the mouse S100A9 recombinant protein, and the mice were divided into five groups: Sham, SAH+vehicle, SAH+rS100A9, KO-SAH, and KO-SAH+rS100A9. Western blotting and immunofluorescence staining were performed to detect the expression of inflammatory factors (IL-18 and IL-1β). The neurobehavioral score results

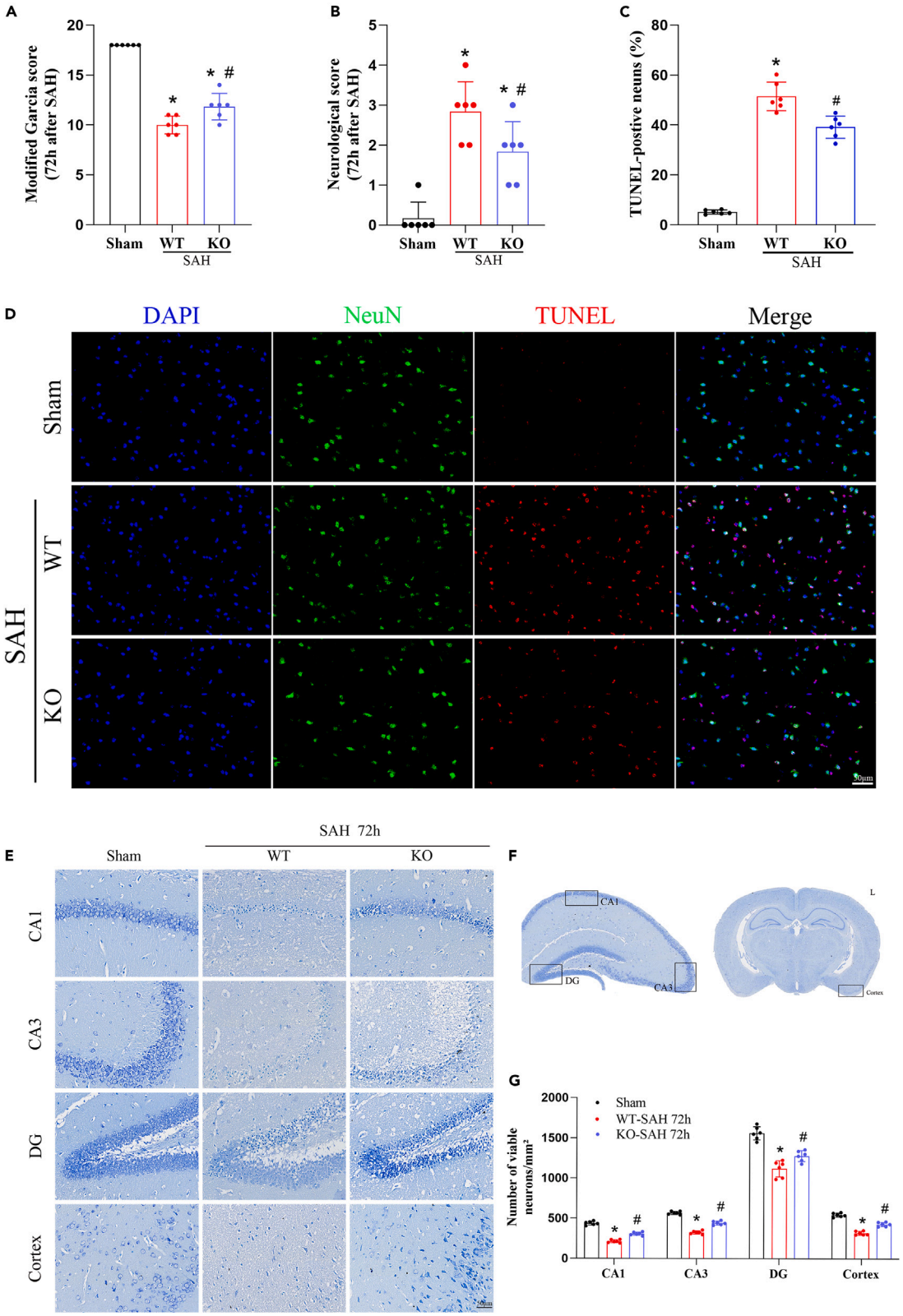
A
Modified Garcia score (72h after SAH)
Sham
WT
KO
SAH
B
Neurological score (72h after SAH)
C
TUNEL-postive neums (%)
D
DAPI
NeuN
TUNEL
Merge
Sham
SAH
WT
KO
E
SAH 72h
Sham
WT
KO
CA1
CA3
DG
Cortex
F
CA1
DG
CA3
L
Cortex
G
Number of viable neurons/mm²
Sham
WT-SAH 72h
KO-SAH 72h
CA1
CA3
DG
Cortex

Figure 4. Effect of S100A9 knockout on cortical and hippocampus neuronal injury at 72 h after SAH

(A and B) The modified Garcia and neurological score of each group. n = 6 per group. *p < 0.05 vs. Sham group; #p < 0.05 vs. WT-SAH group.

(C and D) Representative microphotograph showed the co-localization of TUNEL positive cell (red) with NeuN (green) and quantitative analysis. n = 6 per group. *p < 0.05 vs. Sham group; #p < 0.05 vs. WT-SAH group.

(E–G) Representative picture of Nissl staining and quantitative analysis. n = 6 per group. *p < 0.05 vs. Sham group; #p < 0.05 vs. WT-SAH group. Scale bar, 50 μm. Data were represented as the mean ± SD.

showed that S100A9 administration aggravated neurological damage after SAH in WT mice, and the results were the same in S100A9 knockout mice (Figures 6A and 6B). The results of western blotting showed that S100A9 recombinant protein administration increased the expression of NLRP1, IL-18, and IL-1β after SAH in the mice, while S100A9 knockout significantly reduced the expression and increased again after S100A9 recombinant protein administration (Figures 6C–6G). This result was confirmed by immunofluorescence staining (Figure 6H). In addition, we also confirmed that the administration of S100A9 recombinant protein increased the expression of iba1 (Figure 6C), which may also be one of the underlying mechanisms for the increased expression of inflammatory factors.

Inhibition of S100A9 *in vitro* and *in vivo* SAH models mitigated neuroinflammation by inhibiting the TLR4/MYD88/NF-κB pathway

To further explore the potential mechanism by which S100A9 aggravates neuroinflammation, we examined the expression of related pathways in mice after SAH using western blotting. The results showed that the expression of iNOS, TLR4, MYD88, *p*-IκBα increased after SAH in mice, and the expression of these proteins was significantly increased after the administration of S100A9 recombinant protein. The expression of these proteins decreased after S100A9 knockout and increased after the reapplication of S100A9 recombinant protein. This suggests that S100A9 knockout inhibits the activation of the TLR4/MYD88/NF-κB pathway and reduces the activation of microglia to alleviate inflammation (Figures 7A–7E).

Similarly, we verified the potential mechanism by which S100A9 aggravates neuroinflammation in an *in vitro* SAH model. Western blotting results showed that the expression of iNOS, TLR4, MYD88, *p*-IκBα in BV2 cells increased after hemin stimulation, and their expression continued to increase after the administration of S100A9 recombinant protein. After paquinimod treatment, the expression of these proteins was significantly decreased compared with that in the untreated group, and the expression was increased after re-administration of S100A9 recombinant protein (Figures 7F–7J). We separated cytoplasmic protein and nuclear protein, and then detected the expression of p65 by western blotting, respectively, and the results showed the same trend (Figures 7K and 7L). Immunofluorescence analysis also verified that paquinimod treatment inhibited the nuclear transcription of NF-κB after hemin stimulation, while the addition of S100A9 recombinant protein reactivated the nuclear transcription of NF-κB (Figure 7M).

Neuroinflammation induced by S100A9 can be mitigated by NF-κB inhibitor

To further verify that S100A9 regulates the expression of inflammatory factors through intracellular NF-κB phosphorylation, further nuclear transcription, and finally regulation of inflammatory factors, we introduced the NF-κB inhibitor -PDTC (Pyrrolidinedithiocarbamate). The results show that PDTC can reduce the expression of inflammatory cytokines after SAH and reduce the nuclear transcription of p65 *in vivo* and *in vitro* SAH models (Figures 8A–8T). When PDTC was added in the presence of exogenous S100A9 protein, the expression of related proteins decreased significantly compared with rS100A9 group. This suggests that S100A9 protein is mainly responsible for exacerbating neuroinflammation through TLR4/MYD88/NF-κB pathway.

The level of S100A9 in CSF is closely related to the prognosis of patients with SAH

To determine whether there was any difference between S100A9 protein levels in the CSF of patients with SAH and normal controls, we selected a total of 25 patients with SAH with onset time within 24 h and 15 normal controls. We collected the first CSF sample at admission, for ELISA, and the results showed that the concentration of S100A9 protein in the CSF of patients with SAH with onset time ≤24 h was significantly higher than that of the control group (Figure 9A). To further clarify the changes in S100A9 concentration in the CSF of patients with SAH over time, data from 10 patients were consecutively collected. The results showed that the concentration of S100A9 in the CSF of patients with SAH increased with time after the onset of SAH (Figure 9B), and stabilized after 4–7 days, with no significant difference between 4–7 days and 8–14 days ($p > 0.05$).

In addition, to understand whether there is a correlation between S100A9 concentration in the CSF and short-term outcomes in patients with SAH, we collected the mRS scores of the previous 25 patients at discharge. We graded the mRS Scores as 0–2 (favorable outcome) and 3–6 (unfavorable outcome). The horizontal boxplot showed that the higher the concentration of S100A9 protein in the CSF of patients with onset time ≤24 h, the worse the prognosis of the patients at discharge (Figure 9C).

DISCUSSION

The S100 family of proteins were initially discovered as neuroproteins in the bovine brain in 1965. S100A8, S100A9, and S100A12 are present in inflamed tissues, with neutrophils and monocytes being the primary cell types that contain these proteins.[22] Previous research has established that S100A9 is linked to various diseases, with the inflammatory response serving as the central hub, including inflammation caused by infection,[23] metabolic inflammation,[24] inflammation resulting from immune system dysfunction,[25–27] inflammation caused by degenerative diseases,[28–30] and inflammation-related to neurodegenerative diseases.[31] The gene S100A9 exhibits high expression in glial cells; however, its function in numerous nervous system diseases remains unclear.

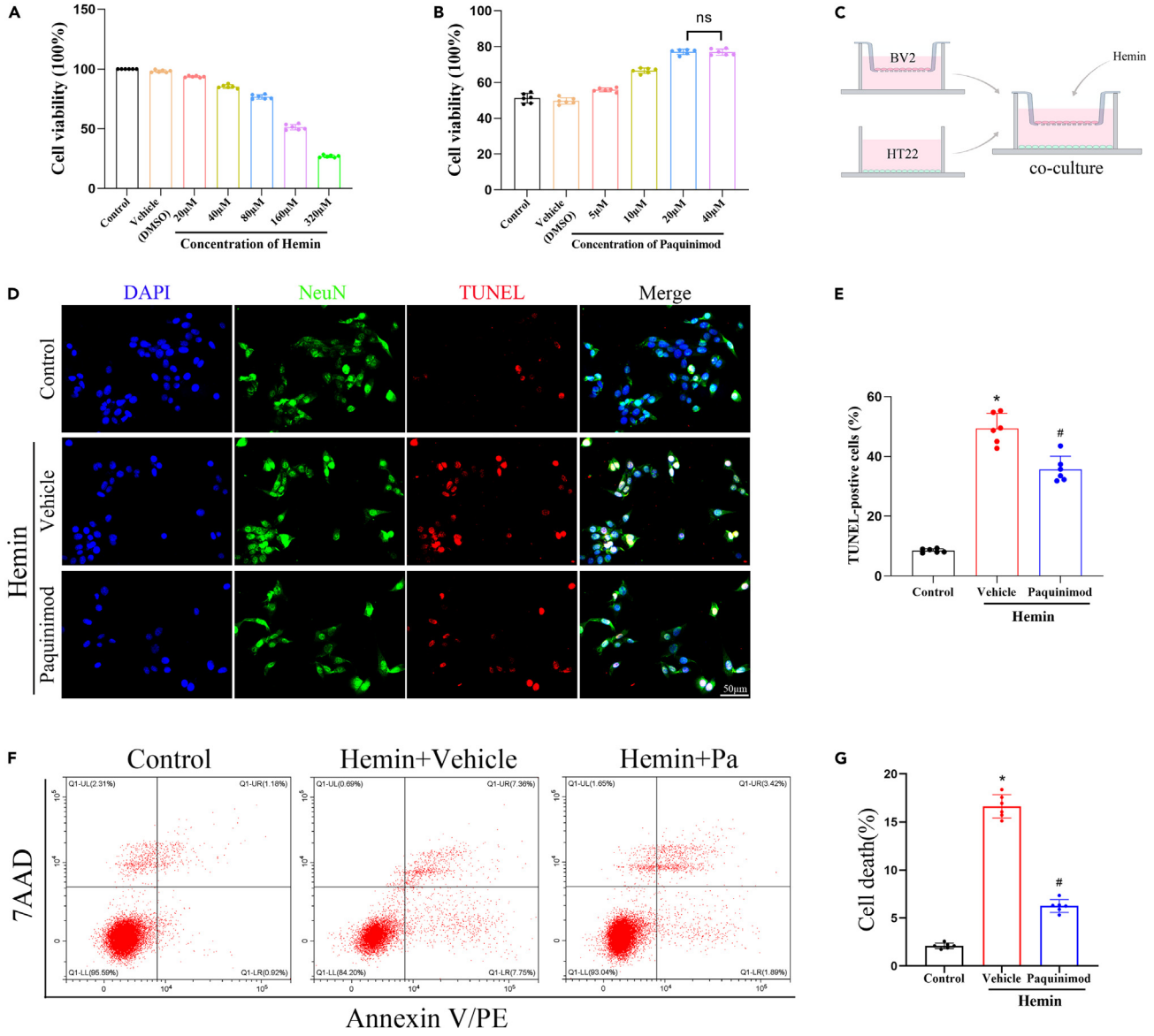

Figure 5. Paquinimod can inhibit hemin-induced neuronal apoptosis

(A and B) CCK-8 results showed that the cell viability decreased significantly after treatment with hemin (160 mmol/L). Paquinimod (20 μmol/L) rescued the process. n = 6 per group.

(C–E) Representative microphotograph showed the co-localization of TUNEL positive cell (red) with NeuN (green) and quantitative analysis. n = 6 per group. *p < 0.05 vs. control group; #p < 0.05 vs. hemin+vehicle group.

(F and G) Representative flow cytometry images of HT22 cells, apoptotic cells represented by 7-AAD+/Annexin V+ ratio. n = 6 per group. *p < 0.05 vs. control group; #p < 0.05 vs. hemin+vehicle group. Scale bar, 50 μm. Data were represented as the mean ± SD.

To address this knowledge gap, we utilized a mouse SAH model and implemented S100A9 knockout to investigate the role of S100A9 in SAH. Our findings indicate that S100A9 knockout mice exhibited improved performance following SAH, as evidenced by significantly enhanced relevant scores in comparison to WT (wild type) mice. This was corroborated by assessment of brain edema and H&E staining post-SAH. Furthermore, our Nissl and TUNEL staining results demonstrate that S100A9 knockout mitigated neuronal apoptosis and improved short-term outcomes (72 h) in the context of SAH model. Our investigation revealed that S100A9 exacerbates brain injury by eliciting an inflammatory response. Additionally, we investigated the mechanism by which S100A9 activates the TLR4/MYD88 pathway to phosphorylate p65 and nuclear transcription, ultimately leading to microglial activation and the release of inflammatory factors. EBI, which encompasses pathological events occurring within 72 h of SAH onset, can be attributed to various factors such as mechanical injury,[32] vascular disruption,[33] and hippocampal injury.[34] In order to examine the correlation between EBI and S100A9, an investigation was conducted to determine if the

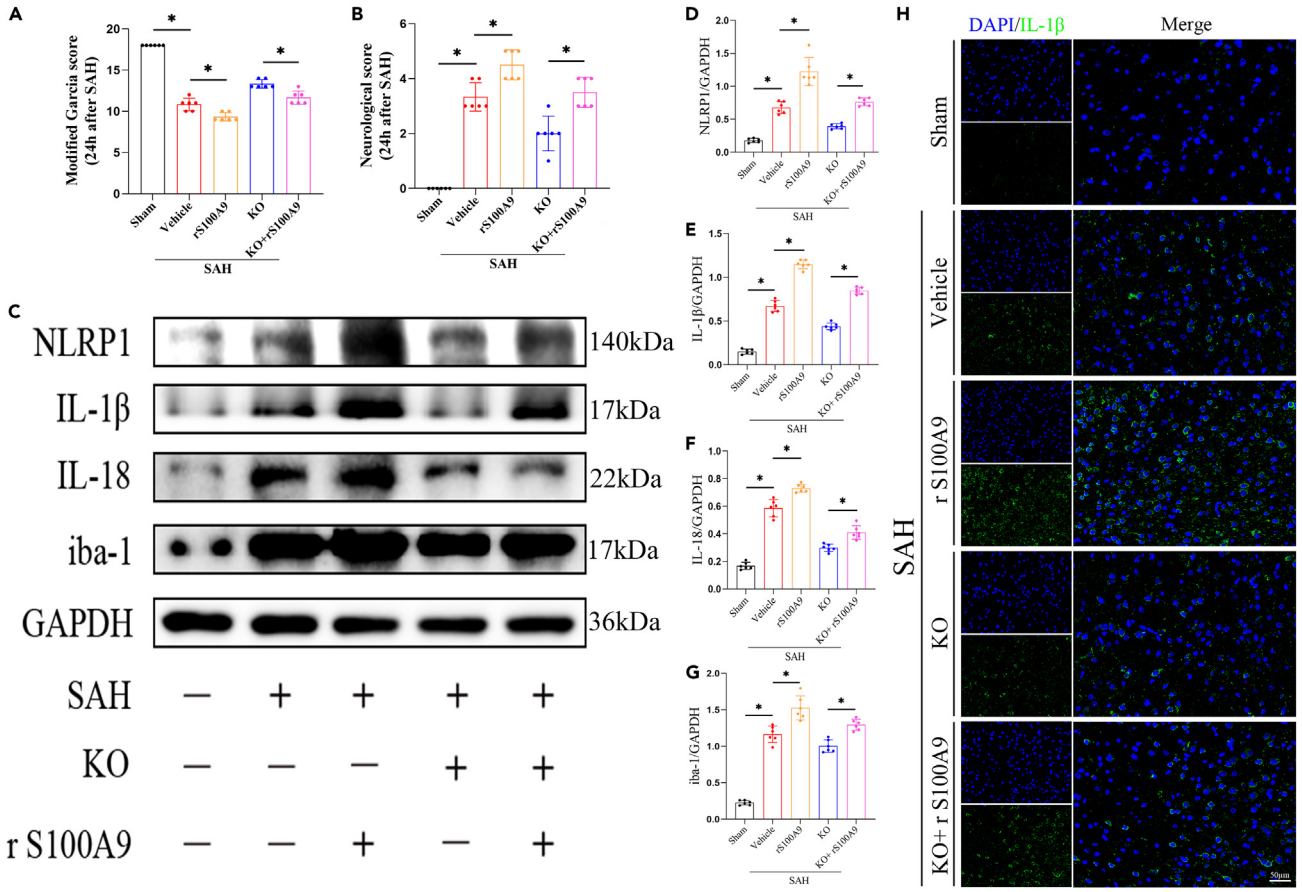

Figure 6. S100A9 aggravates neuroinflammation after SAH

(A and B) Modified Garcia and neurological scores of each group. n = 6 per group.

(C–G) Representative images and quantitative analysis of western blotting for NLRP1 inflammasome, inflammation-related proteins and microglial markers. n = 6 per group.

(H) Representative immunofluorescence images of inflammatory factors. Scale bar, 50 μm. *p < 0.05. Data were represented as the mean ± SD.

expression of S100A9 in the cerebrospinal fluid (CSF) of patients was elevated. CSF samples were collected from patients within 24 h of onset, either prior to or following treatment. Through the use of ELISA, it was discovered that the concentration of S100A9 in the CSF of patients with SAH was generally higher than that of normal controls, despite being lower. However, it should be noted that S100A9 was not entirely absent from the CSF of the normal control group. This suggests that the human body has the ability to secrete a modest amount of S100A9 protein under physiological conditions, which confers a degree of protective benefit. However, when the body is subjected to external stimuli, a significant amount of S100A9 protein is secreted, which functions more as a "molecule of harm". This secretion rate increases over time before eventually stabilizing. Furthermore, the concentration of S100A9 protein is positively associated with the short-term prognosis of individuals with SAH. These findings suggest a robust correlation between S100A9 protein and SAH.[35] Immunofluorescence staining was employed to ascertain the distribution of S100A9 in nerve cells within brain tissue following SAH. The findings revealed a greater expression of S100A9 in microglia, indicating their pivotal role in linking SAH to S100A9 expression. Notably, S100A9 knockout mice exhibited superior neurological scores post-SAH in comparison to their wild-type counterparts. It is widely acknowledged that the hippocampus, a region of the brain, is responsible for all cognitive and emotional functions in humans and possesses remarkable plasticity.[36] H&E staining showed that S100A9 knockout mice had less brain edema and neuronal degeneration in the ipsilateral cortex and hippocampus. Apoptosis, programmed cell death, is a process that occurs in multicellular organisms and is characterized by cell shrinkage, nuclear fragmentation, and chromatin condensation.[37] These changes were observed using Nissl staining, especially in the ipsilateral cortex and hippocampus (CA1, CA3, and DG) after SAH. In addition, S100A9 knockdown significantly improved this phenomenon, as confirmed by TUNEL staining. After SAH, heme produced by the degradation of blood entering the subarachnoid space can activate microglia via TLR4 receptors, thereby inducing a proinflammatory cascade.[38–40] Paquinimod is a specific S100A9 inhibitor, and studies have shown that paquinimod competes with TLR4 and RAGE for the same binding region of calprotectin and does not directly regulate S100A9 protein expression. Therefore, we used hemin to construct an *in vitro* SAH model. Through the co-culture model of BV2 and HT22 cells, it was verified that the number of apoptotic cells reduced significantly after the addition of the S100A9 specific inhibitor, paquinimod, indicating that paquinimod has a protective effect on HT22 cells.

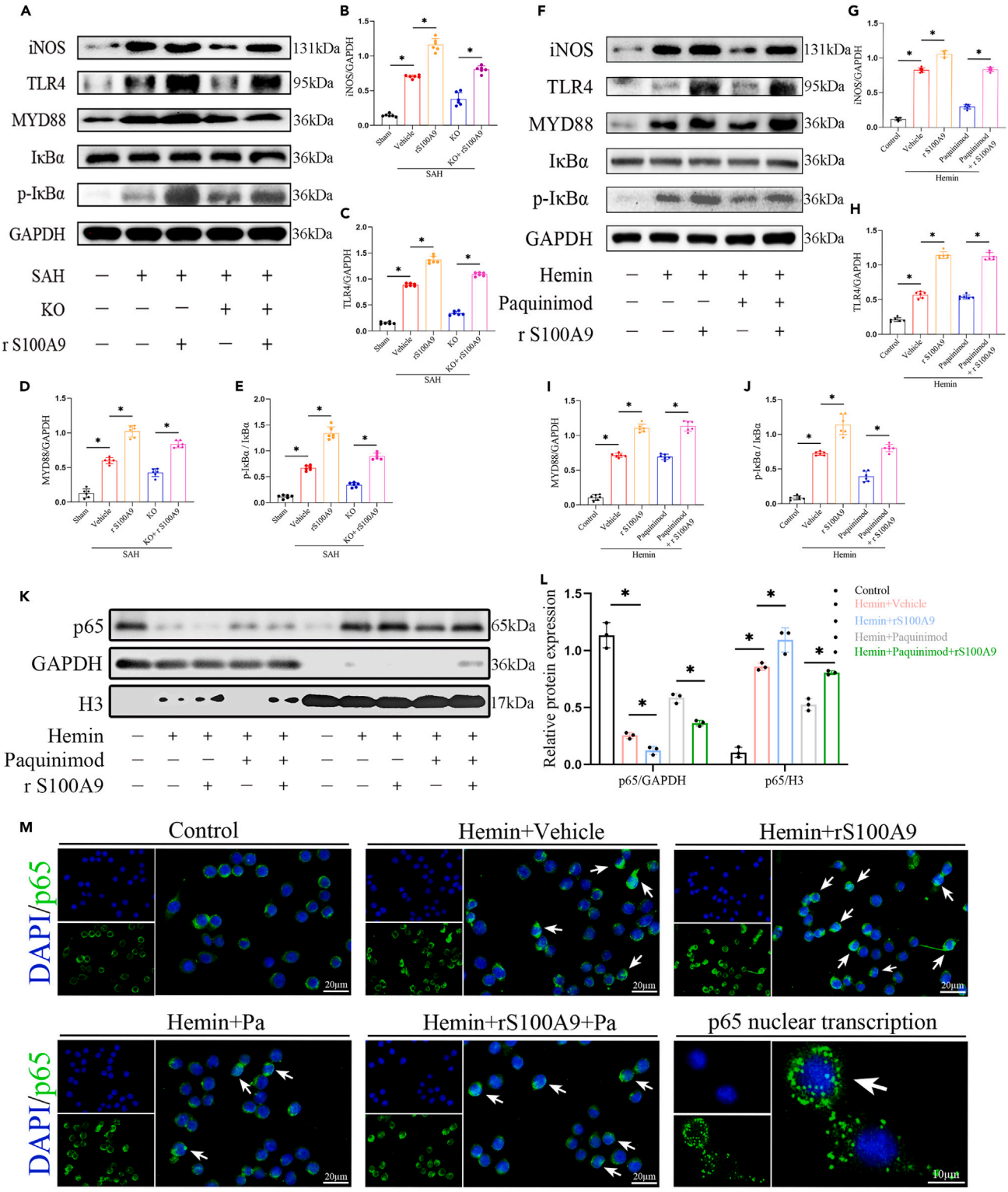

Figure 7. S100A9 induces neuroinflammation by activating the TLR4/MYD88/NF-κB pathway

(A–E) Western blotting and quantitative analyses of iNOS, TLR4, MYD88, IκBα, *p*-IκBα, p65, and p-p65 expression *in vivo* SAH model.

(F–L) Western blotting and quantitative analyses of iNOS, TLR4, MYD88, IκBα, *p*-IκBα, p65 expression *in vitro* SAH model.

(M) Representative immunofluorescence images showed that Paquinimod inhibited nuclear transcription in different groups, and representative images of nuclear transcription. n = 6 per group. Scale bar, 50/20 μm. *p < 0.05. Data were represented as the mean ± SD.

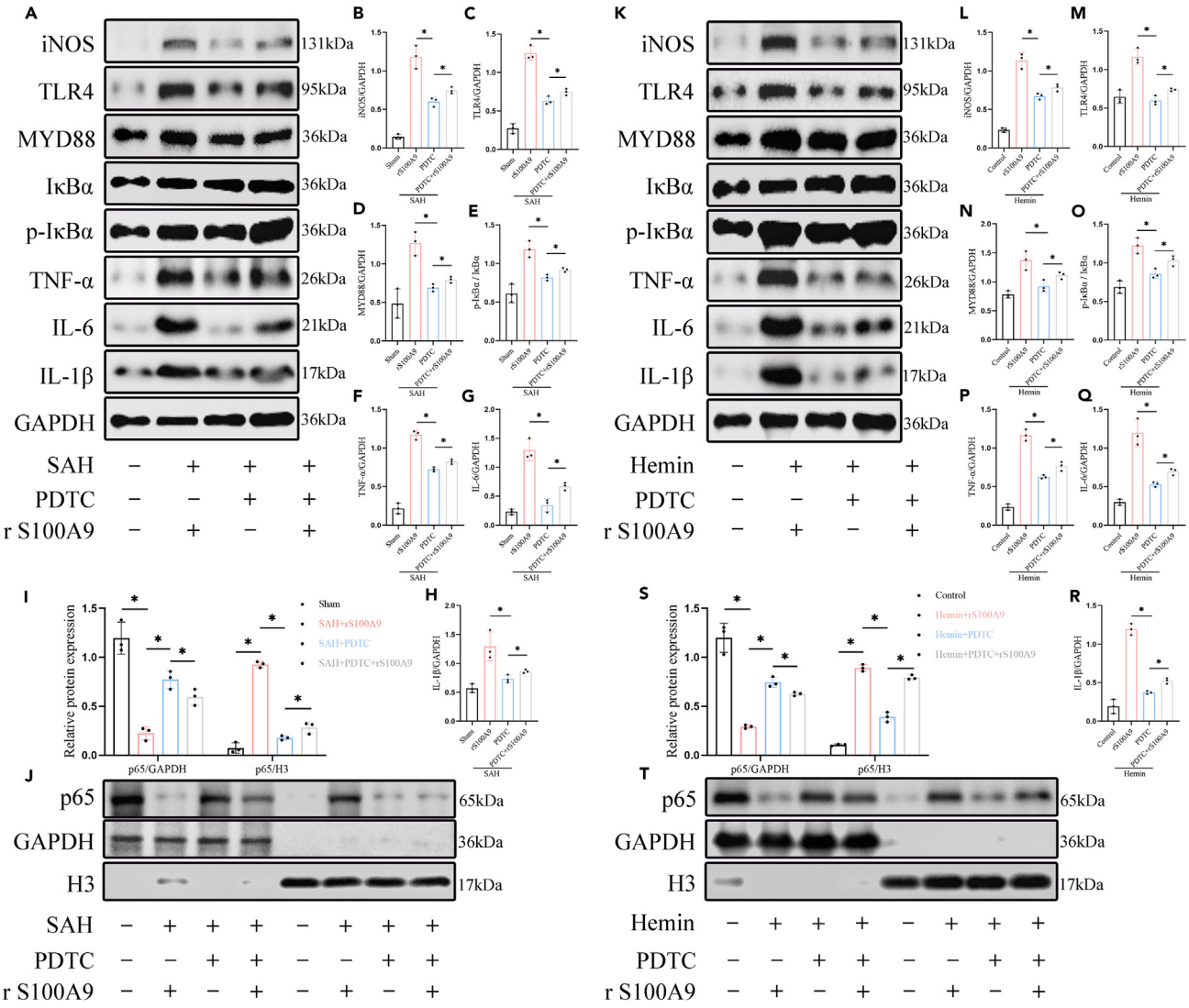

Figure 8. Inhibition of NF-κB phosphorylation alleviates S100A9-induced neuroinflammation

(A–J) Western blotting and quantitative analyses of iNOS, TLR4, MYD88, IκBα, *p*-IκBα, p65, and inflammatory factor expression *in vivo* SAH model.

(K–T) Western blotting and quantitative analyses of iNOS, TLR4, MYD88, IκBα, *p*-IκBα, p65, and inflammatory factor expression *in vitro* SAH model.

Neuroinflammation, mainly mediated by microglial activation and the recruitment of immune cells, is one of the key drivers of EBI after SAH.[41] Short-term prognosis after SAH can be improved by inhibiting neuroinflammation.[42–45] Previous studies have shown that inhibiting IL-6 expression can help relieve cerebral artery spasm and improve nerve damage.[46] Activation of microglia and M1 polarization after SAH were demonstrated by increased levels of iNOS and IL-1β.[47] We further explored the relationship between S100A9 and inflammation by intracerebroventricular injection of the S100A9 recombinant protein. Our study showed that S100A9 knockdown reduced the expression of inflammatory factors in brain tissue after SAH, and the levels of inflammatory factors and microglia marker iba1 were increased again after the addition of S100A9 recombinant protein, suggesting that S100A9 aggravates neuroinflammation after SAH under certain conditions. NF-κB is an important nuclear transcription factor that responds to cells stress and cytokines. When the NF-κB signaling pathway is activated by an upstream signal, the NF-κB complex p65 subunit is released and is further phosphorylated, combined with DNA in the nucleus, and it initiates the transcription of inflammatory factors.[48] Our study showed that the levels of TLR4, MYD88, *p*-IκBα, p-p65, and nuclear translocation of p65 were increased after SAH, which could be inhibited by S100A9 knockdown or paquinimod administration, and intervention with S100A9 recombinant protein could increase the expression levels of these genes again.

In addition, we also observed the activation of NLRP1, an inflammasome. The structure of NLRP1 is different between mice and humans, which makes its function different between different species and adds complexity to our study of NLRP1. NLRP1 has shown different effects in previous studies, for example, it can regulate the composition of intestinal microorganisms and play a role in protecting intestinal mucosa. On the other

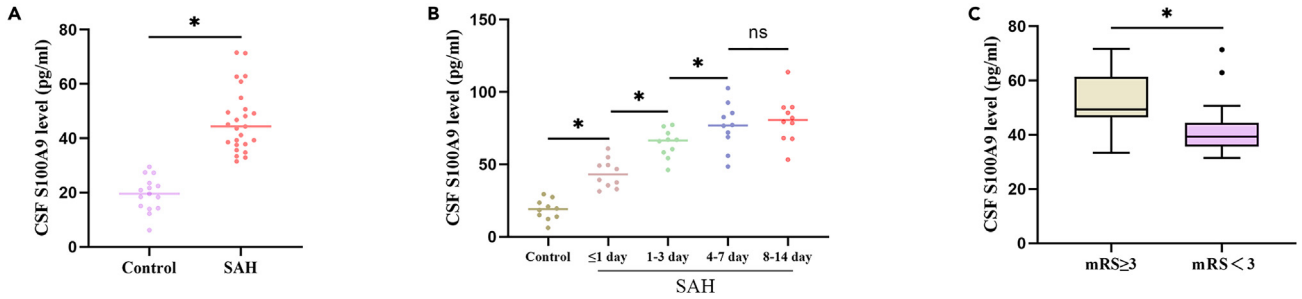

Figure 9. The concentration of S100A9 protein in cerebrospinal fluid (CSF) of patients with SAH, it changes with time and it correlates with short-term prognosis

(A) The levels of S100A9 were detected by ELISA in CSF samples from control and patients with SAH.

(B) The change trend of S100A9 in CSF of patients with SAH with time.

(C) Horizontal boxplot of S100A9 concentration in CSF and mRS at discharge in patients with SAH. *p < 0.05. Data were represented as the mean ± SD.

hand, it can also cause nervous disorders, heart and lung diseases, and tumors by promoting inflammation. We found that NLRP1 is closely related to S100A9 and SAH, but we did not further explore the underlying mechanism, which may be a problem for us to solve in the future.

In our study, S100A9 can promote microglial M1 polarization by promoting TLR4/MYD88/NF-κB pathway activation, activating NLRP1, and promoting neuroinflammation. S100A9 knockdown can reduce early brain injury after SAH and improve short-term prognosis. Therefore, S100A9 inhibitors may be therapeutic targets for alleviating early brain injury after SAH.

Limitations of the study

Our results confirmed that S100A9 knockout could ameliorate early brain injury after SAH by reducing neuroinflammation and NLRP1 inflammasome activation by inhibiting the TLR4/MYD88/NF-κB pathway activation. However, our study had certain limitations. In previous studies, S100A9 was shown to have different effects—proinflammatory or anti-inflammatory,[49] and we did not further explore the conditions under which S100A9 may manifest as an anti-inflammatory molecule after SAH. Second, the *in vivo* SAH process is complex, and the *in vitro* model we established cannot fully simulate it. Finally, whether S100A9 mediates inflammation via other receptor proteins has not been discussed. We only targeted the TLR4 receptor protein; hence, other pathway mechanisms remain to be elucidated.

STAR★METHODS

Detailed methods are provided in the online version of this paper and include the following:

- KEY RESOURCES TABLE
- RESOURCE AVAILABILITY
  - Lead contact
  - Materials availability
  - Data and code availability
- EXPERIMENTAL MODEL AND STUDY PARTICIPANT DETAILS
  - Ethics approval
  - Additional Resources
  - Animals
  - Human cerebrospinal fluid samples
- METHOD DETAILS
  - Data collection
  - SAH animal model
  - Assessment of SAH grade
  - Experimental design
  - Experiment 1
  - Experiment 2
  - Experiment 3
  - Experiment 4
  - Experiment 5
  - ELISA detection
  - Intraventricular injection
  - Brain edema measurement
  - Behavioral analysis

- Nissl and H&E staining
- Immunofluorescence and TUNEL staining
- *In vitro* SAH model
- Cell viability assay
- Flow cytometry
- Western Blot analysis

- QUANTIFICATION AND STATISTICAL ANALYSIS

SUPPLEMENTAL INFORMATION

Supplemental information can be found online at https://doi.org/10.1016/j.isci.2024.109165.

ACKNOWLEDGMENTS

This work was supported by National Natural Science Foundation of China (grant/award number: 81971870, 82172173 to M.L.).

AUTHOR CONTRIBUTIONS

G.W. and K.H. jointly completed the experiment and wrote the original draft of this study. Q.T., Y.G., and C.L. processed the data, Z.L. collected the data, G.W., K.H., Z.Y., Z.Z., and M.L. designed the study, M.L. contributed to the project administration.

DECLARATION OF INTERESTS

The authors declare no competing interests.

Received: September 26, 2023
Revised: December 3, 2023
Accepted: February 5, 2024
Published: February 9, 2024

REFERENCES

1. Bian, L.-H., Liu, Y.-F., Nichols, L.T., Wang, C.-X., Wang, Y.-L., Liu, G.-F., Wang, W.-J., and Zhao, X.-Q. (2012). Epidemiology of subarachnoid hemorrhage, patterns of management, and outcomes in China: a hospital-based multicenter prospective study. CNS Neurosci. Ther. *18*, 895–902.
2. Stienen, M.N., Germans, M., Burkhardt, J.-K., Neidert, M.C., Fung, C., Bervini, D., Zumofen, D., Röthlisberger, M., Marbacher, S., Maduri, R., et al. (2018). Predictors of In-Hospital Death After Aneurysmal Subarachnoid Hemorrhage: Analysis of a Nationwide Database (Swiss SOS [Swiss Study on Aneurysmal Subarachnoid Hemorrhage]). Stroke *49*, 333–340.
3. Laurent, D., Small, C., Lucke-Wold, B., Dodd, W.S., Chalouhi, N., Hu, Y.C., Hosaka, K., Motwani, K., Martinez, M., Polifka, A., et al. (2022). Understanding the genetics of intracranial aneurysms: A primer. Clin. Neurol. Neurosurg. *212*, 107060.
4. Caner, B., Hou, J., Altay, O., Fujii, M., and Zhang, J.H. (2012). Transition of research focus from vasospasm to early brain injury after subarachnoid hemorrhage. J. Neurochem. *123*, 12–21.
5. Cahill, J., and Zhang, J.H. (2009). Subarachnoid hemorrhage: is it time for a new direction? Stroke *40*, S86–S87.
6. Xu, P., Hong, Y., Xie, Y., Yuan, K., Li, J., Sun, R., Zhang, X., Shi, X., Li, R., Wu, J., et al. (2021). TREM-1 Exacerbates Neuroinflammatory Injury via NLRP3 Inflammasome-Mediated Pyroptosis in Experimental Subarachnoid Hemorrhage. Transl. Stroke Res. *12*, 643–659.
7. Ruchika, F., Shah, S., Delawan, M., Durga, N., and Lucke-Wold, B. (2023). Cytokines and subarachnoid hemorrhage. In Vitro Diagn *1*.
8. Rass, V., and Helbok, R. (2019). Early Brain Injury After Poor-Grade Subarachnoid Hemorrhage. Curr. Neurol. Neurosci. Rep. *19*, 78.
9. Tabarestani, A., Patel, A., Reddy, A., Sharaf, R., and Lucke-Wold, B. (2023). Vasospasm Management Strategies. Int. J. Med. Pharm. Res. *4*, 150–160.
10. Schneider, U.C., Davids, A.-M., Brandenburg, S., Müller, A., Elke, A., Magrini, S., Atangana, E., Turkowski, K., Finger, T., Gutenberg, A., et al. (2015). Microglia inflict delayed brain injury after subarachnoid hemorrhage. Acta Neuropathol. *130*, 215–231.
11. Ma, C., Zhou, W., Yan, Z., Qu, M., and Bu, X. (2015). Toll-like receptor 4 (TLR4) is correlated with delayed cerebral ischemia (DCI) and poor prognosis in aneurysmal subarachnoid hemorrhage. J. Neurol. Sci. *359*, 67–71.
12. Okada, T., and Suzuki, H. (2017). Toll-like receptor 4 as a possible therapeutic target for delayed brain injuries after aneurysmal subarachnoid hemorrhage. Neural Regen. Res. *12*, 193–196.
13. Weiland, J., Beez, A., Westermaier, T., Kunze, E., Sirén, A.L., and Lilla, N. (2021). Neuroprotective Strategies in Aneurysmal Subarachnoid Hemorrhage (aSAH). Int. J. Mol. Sci. *22*, 5442.
14. Li, Y., Zhang, L., Tang, J., Yang, X., Huang, J., Zhu, T., Zhao, F., Li, S., Li, X., Qu, Y., and Mu, D. (2019). Role of toll-like receptor 4 in the regulation of the cell death pathway and neuroinflammation. Brain Res. Bull. *148*, 79–90.
15. Buchanan, M.M., Hutchinson, M., Watkins, L.R., and Yin, H. (2010). Toll-like receptor 4 in CNS pathologies. J. Neurochem. *114*, 13–27.
16. Li, L., Acioglu, C., Heary, R.F., and Elkabes, S. (2021). Role of astroglial toll-like receptors (TLRs) in central nervous system infections, injury and neurodegenerative diseases. Brain Behav. Immun. *91*, 740–755.
17. Roh, J.S., and Sohn, D.H. (2018). Damage-Associated Molecular Patterns in Inflammatory Diseases. Immune Netw. *18*, e27.
18. Wang, S., Song, R., Wang, Z., Jing, Z., Wang, S., and Ma, J. (2018). S100A8/A9 in Inflammation. Front. Immunol. *9*, 1298.
19. Pruenster, M., Vogl, T., Roth, J., and Sperandio, M. (2016). S100A8/A9: From basic science to clinical application. Pharmacol. Ther. *167*, 120–131.
20. Liu, C., Yao, K., Tian, Q., Guo, Y., Wang, G., He, P., Wang, J., Wang, J., Zhang, Z., and Li, M. (2023). CXCR4-BTK axis mediate pyroptosis and lipid peroxidation in early brain injury after subarachnoid hemorrhage via NLRP3 inflammasome and NF-κB pathway. Redox Biol. *68*, 102960.
21. Tupik, J.D., Nagai-Singer, M.A., and Allen, I.C. (2020). To protect or adversely affect? The dichotomous role of the NLRP1 inflammasome in human disease. Mol. Aspect. Med. *76*, 100858.
22. Foell, D., Wittkowski, H., Vogl, T., and Roth, J. (2007). S100 proteins expressed in phagocytes: a novel group of damage-associated molecular pattern molecules. J. Leukoc. Biol. *81*, 28–37.
23. De Jong, H.K., Achouiti, A., Koh, G.C.K.W., Parry, C.M., Baker, S., Faiz, M.A., van Dissel,

J.T., Vollaard, A.M., van Leeuwen, E.M.M., Roelofs, J.J.T.H., et al. (2015). Expression and function of S100A8/A9 (calprotectin) in human typhoid fever and the murine Salmonella model. PLoS Neglected Trop. Dis. *9*, e0003663.
24. Oliva, K., Barker, G., Rice, G.E., Bailey, M.J., and Lappas, M. (2013). 2D-DIGE to identify proteins associated with gestational diabetes in omental adipose tissue. J. Endocrinol. *218*, 165–178.
25. Tydén, H., Lood, C., Gullstrand, B., Jönsen, A., Ivars, F., Leanderson, T., and Bengtsson, A.A. (2017). Pro-inflammatory S100 proteins are associated with glomerulonephritis and anti-dsDNA antibodies in systemic lupus erythematosus. Lupus *26*, 139–149.
26. Takama, H., Sugiura, K., Ogawa, Y., Muro, Y., and Akiyama, M. (2013). Possible roles of barrier-to-autointegration factor 1 in regulation of keratinocyte differentiation and proliferation. J. Dermatol. Sci. *71*, 100–106.
27. Lee, D.-G., Woo, J.-W., Kwok, S.-K., Cho, M.-L., and Park, S.-H. (2013). MRP8 promotes Th17 differentiation via upregulation of IL-6 production by fibroblast-like synoviocytes in rheumatoid arthritis. Exp. Mol. Med. *45*, e20.
28. Swindell, W.R., Johnston, A., Xing, X., Little, A., Robichaud, P., Voorhees, J.J., Fisher, G., and Gudjonsson, J.E. (2013). Robust shifts in S100a9 expression with aging: a novel mechanism for chronic inflammation. Sci. Rep. *3*, 1215.
29. van den Bosch, M.H., Blom, A.B., Schelbergen, R.F., Koenders, M.I., van de Loo, F.A., van den Berg, W.B., Vogl, T., Roth, J., van der Kraan, P.M., and van Lent, P.L. (2016). Alarmin S100A9 Induces Proinflammatory and Catabolic Effects Predominantly in the M1 Macrophages of Human Osteoarthritic Synovium. J. Rheumatol. *43*, 1874–1884.
30. Rosenberg, J.H., Rai, V., Dilisio, M.F., Sekundiak, T.D., and Agrawal, D.K. (2017). Increased expression of damage-associated molecular patterns (DAMPs) in osteoarthritis of human knee joint compared to hip joint. Mol. Cell. Biochem. *436*, 59–69.
31. Wang, C., Klechikov, A.G., Gharibyan, A.L., Wärmländer, S.K.T.S., Jarvet, J., Zhao, L., Jia, X., Narayana, V.K., Shankar, S.K., Olofsson, A., et al. (2014). The role of pro-inflammatory S100A9 in Alzheimer's disease amyloid-neuroinflammatory cascade. Acta Neuropathol. *127*, 507–522.
32. Fujii, M., Yan, J., Rolland, W.B., Soejima, Y., Caner, B., and Zhang, J.H. (2013). Early brain injury, an evolving frontier in subarachnoid hemorrhage research. Transl. Stroke Res. *4*, 432–446.
33. Li, Y., Wu, P., Bihl, J.C., and Shi, H. (2020). Underlying Mechanisms and Potential Therapeutic Molecular Targets in Blood-Brain Barrier Disruption after Subarachnoid Hemorrhage. Curr. Neuropharmacol. *18*, 1168–1179.
34. Han, S.M., Wan, H., Kudo, G., Foltz, W.D., Vines, D.C., Green, D.E., Zoerle, T., Tariq, A., Brathwaite, S., D'Abbondanza, J., et al. (2014). Molecular alterations in the hippocampus after experimental subarachnoid hemorrhage. J. Cerebr. Blood Flow Metabol. *34*, 108–117.
35. Provencio, J.J., Altay, T., Smithason, S., Moore, S.K., and Ransohoff, R.M. (2011). Depletion of Ly6G/C(+) cells ameliorates delayed cerebral vasospasm in subarachnoid hemorrhage. J. Neuroimmunol. *232*, 94–100.
36. Zhou, H., Chen, L., Gao, X., Luo, B., and Chen, J. (2012). Moderate traumatic brain injury triggers rapid necrotic death of immature neurons in the hippocampus. J. Neuropathol. Exp. Neurol. *71*, 348–359.
37. Dong, Y., Fan, C., Hu, W., Jiang, S., Ma, Z., Yan, X., Deng, C., Di, S., Xin, Z., Wu, G., et al. (2016). Melatonin attenuated early brain injury induced by subarachnoid hemorrhage via regulating NLRP3 inflammasome and apoptosis signaling. J. Pineal Res. *60*, 253–262.
38. Zheng, Z.V., Lyu, H., Lam, S.Y.E., Lam, P.K., Poon, W.S., and Wong, G.K.C. (2020). The Dynamics of Microglial Polarization Reveal the Resident Neuroinflammatory Responses After Subarachnoid Hemorrhage. Transl. Stroke Res. *11*, 433–449.
39. Blackburn, S.L., Kumar, P.T., McBride, D., Zeineddine, H.A., Leclerc, J., Choi, H.A., Dash, P.K., Grotta, J., Aronowski, J., Cardenas, J.C., and Doré, S. (2018). Unique Contribution of Haptoglobin and Haptoglobin Genotype in Aneurysmal Subarachnoid Hemorrhage. Front. Physiol. *9*, 592.
40. Lu, Y., Zhang, X.-S., Zhang, Z.-H., Zhou, X.-M., Gao, Y.-Y., Liu, G.-J., Wang, H., Wu, L.-Y., Li, W., and Hang, C.-H. (2018). Peroxiredoxin 2 activates microglia by interacting with Toll-like receptor 4 after subarachnoid hemorrhage. J. Neuroinflammation *15*, 87.
41. Khey, K.M.W., Huard, A., and Mahmoud, S.H. (2020). Inflammatory Pathways Following Subarachnoid Hemorrhage. Cell. Mol. Neurobiol. *40*, 675–693.
42. Xu, H., Li, J., Wang, Z., Feng, M., Shen, Y., Cao, S., Li, T., Peng, Y., Fan, L., Chen, J., et al. (2017). Methylene blue attenuates neuroinflammation after subarachnoid hemorrhage in rats through the Akt/GSK-3β/MEF2D signaling pathway. Brain Behav. Immun. *65*, 125–139.
43. Xu, W., Li, T., Gao, L., Zheng, J., Yan, J., Zhang, J., and Shao, A. (2019). Apelin-13/APJ system attenuates early brain injury via suppression of endoplasmic reticulum stress-associated TXNIP/NLRP3 inflammasome activation and oxidative stress in a AMPK-dependent manner after subarachnoid hemorrhage in rats. J. Neuroinflammation *16*, 247.
44. Tian, Q., Guo, Y., Feng, S., Liu, C., He, P., Wang, J., Han, W., Yang, C., Zhang, Z., and Li, M. (2022). Inhibition of CCR2 attenuates neuroinflammation and neuronal apoptosis after subarachnoid hemorrhage through the PI3K/Akt pathway. J. Neuroinflammation *19*, 312.
45. Tian, Q., Li, Y., Feng, S., Liu, C., Guo, Y., Wang, G., Wei, H., Chen, Z., Gu, L., and Li, M. (2023). Inhibition of CCR1 attenuates neuroinflammation via the JAK2/STAT3 signaling pathway after subarachnoid hemorrhage. Int. Immunopharm. *125*, 111106.
46. Lucke-Wold, B., Dodd, W., Motwani, K., Hosaka, K., Laurent, D., Martinez, M., Dugan, V., Chalouhi, N., Lucke-Wold, N., Barpujari, A., et al. (2022). Investigation and modulation of interleukin-6 following subarachnoid hemorrhage: targeting inflammatory activation for cerebral vasospasm. J. Neuroinflammation *19*, 228.
47. Xiong, X.-Y., Liu, L., and Yang, Q.-W. (2016). Functions and mechanisms of microglia/macrophages in neuroinflammation and neurogenesis after stroke. Prog. Neurobiol. *142*, 23–44.
48. Zeng, J., Chen, Y., Ding, R., Feng, L., Fu, Z., Yang, S., Deng, X., Xie, Z., and Zheng, S. (2017). Isoliquiritigenin alleviates early brain injury after experimental intracerebral hemorrhage via suppressing ROS- and/or NF-κB-mediated NLRP3 inflammasome activation by promoting Nrf2 antioxidant pathway. J. Neuroinflammation *14*, 119.
49. Achouiti, A., Vogl, T., Van der Meer, A.J., Stroo, I., Florquin, S., de Boer, O.J., Roth, J., Zeerleder, S., van 't Veer, C., de Vos, A.F., and van der Poll, T. (2015). Myeloid-related protein-14 deficiency promotes inflammation in staphylococcal pneumonia. Eur. Respir. J. *46*, 464–473.
50. Nishikawa, H., Liu, L., Nakano, F., Kawakita, F., Kanamaru, H., Nakatsuka, Y., Okada, T., and Suzuki, H. (2018). Modified Citrus Pectin Prevents Blood-Brain Barrier Disruption in Mouse Subarachnoid Hemorrhage by Inhibiting Galectin-3. Stroke *49*, 2743–2751.
51. Silva, C.R., Melo, B.M.S., Silva, J.R., Lopes, A.H., Pereira, J.A., Cecilio, N.T., Berlink, J., Souza, G.G., Lucas, G., Vogl, T., et al. (2020). S100A9 plays a pivotal role in a mouse model of herpetic neuralgia via TLR4/TNF pathway. Brain Behav. Immun. *88*, 353–362.
52. Gao, S., Zhou, L., Lu, J., Fang, Y., Wu, H., Xu, W., Pan, Y., Wang, J., Wang, X., Zhang, J., and Shao, A. (2022). Cepharanthine Attenuates Early Brain Injury after Subarachnoid Hemorrhage in Mice via Inhibiting 15-Lipoxygenase-1-Mediated Microglia and Endothelial Cell Ferroptosis. Oxid. Med. Cell. Longev. *2022*, 4295208.

STAR★METHODS

KEY RESOURCES TABLE

REAGENT or RESOURCE	SOURCE	IDENTIFIER
Antibodies		
anti-S100A9	Abcam	ab92507
anti-NLRP1	Proteintech	12256-1-AP
anti-iba1	Abcam	ab283319
anti-NeuN	Abcam	ab104224
anti-TLR4	Bioswamp	PAB47910
anti-MYD88	Bioswamp	PAB47936
anti-TNF-α	Bioswamp	PAB36517
anti-IL-1β	Bioswamp	PAB45925
anti-IL-18	Abcam	ab191860
anti-IL-6	Proteintech	21865-1-AP
anti-IκB-α	Proteintech	10268-1-AP
anti-*p*-IκB-α	Proteintech	82349-1-RR
anti-NF-κB	Proteintech	80979-1-RR
anti-GAPDH	Servicebio	GB15002-100
anti-H3	Servicebio	GB11102-100
Biological samples		
Cerebrospinal fluid from subarachnoid hemorrhage patients	Renmin Hospital of Wuhan University	WDRY2021-K070
Cerebrospinal fluid from normal controls	Renmin Hospital of Wuhan University	WDRY2021-K070
Chemicals, peptides, and recombinant proteins		
Mouse recombinant S100A9 protein	MCE	HY-P74583
NF-κB inhibitor -PDTC	MCE	HY-18738
S100A9 inhibitors- Paquinimod	MCE	ABR25757
Hemin chloride	Sigma	51280
Deposited data		
The GSE79416 dataset	Gene Expression Omnibus (GEO) database	https://www.ncbi.nlm.nih.gov/geo/
Experimental models: Cell lines		
Murine BV2 cells	Procell Life Science&Technology Co.,Ltd.	CL-0493A
Murine HT22 cells	Procell Life Science&Technology Co.,Ltd.	CL-0697
Experimental models: Organisms/strains		
Mouse:C57BL/6J male mice	Hunan SJA Laboratory Animal Co.Ltd.	N/A
Mouse: S100A9$^{-/-}$ male mice	Cyagen Biosciences	KOAIP210728XW3
Software and algorithms		
ImageJ	Schneider et al.	https://imagej.nih.gov/ij/
Prism	GraphPad	https://www.graphpad.com/
R-studio	N/A	https://www.r-project.org/

RESOURCE AVAILABILITY

The GSE79416 dataset can be downloaded from the Gene Expression Omnibus (GEO) database (https://www.ncbi.nlm.nih.gov/geo/).

Lead contact

More detailed resource information can be provided by the lead contact Mingchang Li (mingcli@whu.edu.cn) when necessary.

Materials availability

This study did not generate new unique reagents.

Data and code availability

- All data reported in this paper will be shared by the lead contact upon reasonable request.
- No original code was reported in this study.
- Additional information required to reanalyze the data reported in this paper is available from the lead contact upon request.

EXPERIMENTAL MODEL AND STUDY PARTICIPANT DETAILS

Ethics approval

All animal experiments were approved by the Animal Experiment Center of Wuhan University.

Additional Resources

All samples in this study were approved by the Ethics Committee of Renmin Hospital of Wuhan University (Clinical registration number: WDRY2021-K070).

Animals

Wild-type (WT) C57BL/6J male mice (n = 233, 8–10 weeks of age, 22–25 g) and S100A9-KO mice (n = 98, 8–10 weeks of age, 22–25 g) were used in this study. WT mice were purchased from Hunan SJA Laboratory Animal Co.Ltd. S100A9-KO mice were purchased from Cyagen Biosciences (KOAIP210728XW3; Guangzhou, China). The mice used in this study were bred at the Animal Experimental Center of Renmin Hospital, Wuhan University. All mice had free access to food and water throughout the experiment, and were randomly assigned to groups prior to the start of the experiment. The animal experiments in this study were approved by the Animal Welfare Ethics Review Committee of the Renmin Hospital of Wuhan University.

Human cerebrospinal fluid samples

Cerebrospinal fluid (CSF) was collected from SAH patients. This study was approved by the Ethics Committee of Renmin Hospital of Wuhan University. The data of patients admitted to our hospital from July 2021 to July 2022 were collected. All patients were aged from 18 to 75 years old, and the influencing factors such as gender and age were not considered. Patients with SAH were screened within 24 h of SAH onset. CSF was collected by lumbar puncture or external ventricular drainage in 25 patients and continuously in 10 patients. Normal controls, including but not limited to hydrocephalus, underwent lumbar puncture to collect CSF. All patients with SAH included in the study were scored using the Modified Rankin Scale (mRS) at discharge. All samples were obtained from patients after clinical treatment, and informed consent was obtained from all patients.

METHOD DETAILS

Data collection

The GSE79416 dataset was downloaded from the Gene Expression Omnibus (GEO) database. The gene expression matrix of the GSE79416 dataset was analyzed with the "limma" package in R to obtain DEGs between SAH and Control samples. Briefly, |log2 fold change (FC)|>2 and $p < 0.05$ were set as the selection criteria for DEGs. Then, the results were intersected with PRGs to obtain the DEPRGs. The pheatmap package (version 1.0.12) was used to construct the heatmap of these genes.

SAH animal model

An *in vivo* SAH model was established using a modified single-clip method. Anesthesia was induced with isoflurane at a concentration of 5% before the start of surgery, and the mice were intubated with 2–3% isoflurane during surgery (isoflurane was reduced to 1.5% at the time of puncture). The mice were placed in the supine position, and the skin of the neck was dissected after skin preparation, approximately 1.5–2 cm in length. The common and internal carotid arteries were then temporarily clipped with an aneurysm clip, followed by the delivery of a thread-containing silicone coating from the external carotid artery to the internal carotid artery, after which the clip was released. The thread was then gradually pushed into the brain along the vessel. When little resistance was detected, it was indicative that the bifurcation of the anterior cerebral artery and the middle cerebral artery has been reached, and pierce was continued for 2 mm. The sham group mice were also subjected to the procedures described above, except for puncturing the vessel upon reaching the bifurcation. Vital signs were monitored every 3 min to ensure that the mice did not experience any distress or death. The entire procedure lasted approximately 10–15 min. After recovery from anesthesia, the mice were returned to their cages and were placed in an animal room.

Assessment of SAH grade

All mouse models were graded according to SAH severity. Briefly, the basal cistern was divided into six parts, and each site was scored on a scale of 0–3, according to the amount of subarachnoid hemorrhage. All scores were summed to obtain a total score (maximum score of 18). We excluded mice with a total score <8 from the study.

Experimental design

A total of 331 mice were used in this study, and were subjected to four independent experiments (S1).

Experiment 1

To determine the expression of S100A9 protein in the brain tissue of mice and its major effector cells (after SAH), we randomly divided the mice into different time points (3, 6, 12, 24, and 72 h) after SAH induction. Cerebral cortex tissues ipsilateral to the puncture site were collected at corresponding time points for western blotting, and the distribution of S100A9 protein was determined by double immunofluorescence staining.

Experiment 2

To explore the role of S100A9 in the pathological process after SAH, S100A9 knockout mice were used to establish an SAH model. Mice were divided into sham, WT-SAH, and KO-SAH groups. Neurological function of these mice was evaluated at 24 h after SAH (n = 10). The expression of S100A9 protein in knockout mice was verified by western blotting. The left and right hemispheres of the mice were collected for assessment of brain water content, and hematoxylin and eosin (H&E) staining was performed on the ipsilateral cortex and hippocampus.

Experiment 3

To explore the effect of S100A9 on neuronal injury after SAH, the mice were divided into three groups: Sham, WT-SAH, and KO-SAH. Neurological function was evaluated 72 h after SAH, and neuronal damage was evaluated by TUNEL staining and Nissl staining.

Experiment 4

To explore whether S100A9 aggravates brain injury after SAH and its effect on microglial expression by inducing neuroinflammation as well as the underlying molecular mechanism, mice were divided into the following five groups: sham, SAH+Vehicle, SAH+rS100A9, KO-SAH, and KO-SAH+rS100A9. Neurological function was assessed 24 h after SAH, and cortical tissues were collected for western blotting and immunofluorescence staining to evaluate the expression of inflammatory factors.

Experiment 5

To verify whether S100A9 aggravates neuroinflammation by increasing NF-κB phosphorylation, we introduced NF-κB inhibitor -PDTC (HY-18738, MCE, USA) and intraperitoneally injected PDTC 1h before SAH. The mice were divided mice into sham, SAH+rS100A9, SAH+PDTC, and SAH+rS100A9+PDTC groups. Cortical tissues were collected 24 h after SAH for western blotting to evaluate the expression of related proteins.

ELISA detection

The CSF was stored on ice and immediately subjected to rotational centrifugation. Supernatants were collected and stored in a refrigerator at −80°C until use for enzyme linked immunosorbent assay (ELISA). We used ELISA kits to measure S100A9 (HM11103, Bioswamp, China) levels in human CSF samples, including patients with SAH and normal controls. ELISA was performed on all samples in triplicates according to the manufacturer's instructions.

Intraventricular injection

Intraventricular (i.c.v) stereotactic delivery was performed as described previously.[50] Briefly, intraperitoneal anesthesia was performed with 1% pentobarbital, and the mice were immobilized on a stereoscopic device. A 10 μL microsyringe was inserted into the left lateral ventricle at coordinates of 0.4 mm posterior and 1.0 mm lateral to the prechamber and 3.0 mm inferior to the dural layer. Mouse recombinant S100A9 protein (HY-P74583, MCE, China) was administered at a dose of 100 ng per mouse as previously described.[51] A total volume of 5.0 μL of S100A9 recombinant protein or ddH_2O was injected 1 h before SAH induction at an injection rate of approximately 0.5 μL/min.

Brain edema measurement

At 24 h after SAH, mouse brains were harvested and weighed to obtain wet weight, dried in a constant-temperature oven for 24 h, and weighed again to obtain the dry weight. The percentage of tissue water content was calculated using the formula ([wet weight − dry weight]/wet weight) ×100%.

Behavioral analysis

An uninformed experimenter assessed all neurological scores. The modified Garcia score was used to evaluate the degree of neurological damage 24 and 72 h after SAH modeling. The total score ranged from 1 to 18 points, and the specific scoring criteria included 6 indicators: spontaneous movement (0–3 points), limb symmetry (0–3 points), forelimb extension (0–3 points), climbing (1–3 points), proprioception (1–3 points) and tentaculum reaction (1–3 points). We also cited another neuroethology to assess the extent of short nerve deficits, but did not create new groupings. Scoring was performed to assess appetite, activity, and deficits in mice at 24 and 72 h after SAH modeling. Specific neurological deficits were graded as follows: severe (score = 4 to 6), moderate (score = 2 to 3), mild (score = 1), and no neurological deficit (score = 0).

Nissl and H&E staining

At 24 or 72 h after SAH, the sacrificed mice were perfused with 4% paraformaldehyde (PFA) and cold phosphate-buffered saline (PBS). The whole brain was then harvested and stored in PFA solution for 24 h. Mouse brains were then cut into 5 μm sections at the indicated sites after embedding in paraffin. Finally, Nissl staining was performed using 5% cresyl blue, and the samples were observed using light microscopy by an uninformed experimenter. For H&E staining, samples were prepared in the same way as for Nissl staining, distinguished by the staining, where paraffin sections were immersed in H&E.

Immunofluorescence and TUNEL staining

Mice were transcardially perfused with normal saline and 4% PFA 24 h after SAH. Samples for tissue immunofluorescence were prepared using Nissl staining. For cellular immunofluorescence, we seeded cells in 6-well Transwell plates for co-culture and treated them with hemin to mimic an *in vitro* SAH model.

For immunofluorescence staining of tissues and cells, samples were blocked with 5% fetal bovine serum (FBS) at room temperature for 1 h, then diluted primary antibodies of interest were added and incubated overnight (4°C). On the next day, after washing, the corresponding secondary antibodies were added and the cells were incubated for 1 h at room temperature. The slides were cleaned and sealed with DAPI (4-6-diamidino-2-phenylindole) reagent, followed by automatic fluorescence microscopy. The primary antibodies used were anti-S100A9 (1:100, ab92507, Abcam, USA), anti-iba1 (1:200, ab283319, Abcam, USA), anti-NeuN (1:400, ab104224, Abcam, USA), anti-NF-κB p65 (1:300,80979-1-RR, Proteintech, USA), and anti-IL-1β (1:200, PAB45925, Bioswamp, China). The secondary antibodies were Alexa 488-conjugated and Alexa 594-conjugated (1:400 for iba1, S100A9, NeuN, IL-1β, and p65; ab150080, ab150077, ab150116, ab150113, Abcam, USA), respectively.

TUNEL staining was performed to determine the degree of apoptosis. TUNEL staining was performed according to the manufacturer's instructions (G1502, Servicebio, China). After TUNEL labeling, the samples were counterstained with DAPI to detect nuclei; apoptotic nuclei were stained red.

In vitro SAH model

Murine BV2 and HT22 cells were cultured in Dulbecco's Modified Eagle Medium (DMEM; Procell, China) with 10–15% FBS (Gibco, USA) and 1% penicillin/streptomycin (Gibco, USA).

We stimulated the cells with hemin chloride (Sigma-Aldrich, MO, USA) to mimic the SAH model *in vitro*.[52] Hemin was used to treat BV2 cells, and the subsequent experimental conditions were determined using different treatment times and concentrations. Cells were treated with S100A9 inhibitors (HY-100442, Paquinimod/ABR25757, MCE, China) to mimic an *in vitro* knockout model. Co-cultured cells were randomly assigned into three groups: control, Hemin+Vehicle, and Hemin+Paquinimod. Cells were treated with paquinimod at the same time points as hemin.

Cell viability assay

A cell counting kit-8 (CCK-8; Biosharp, China) was used to detect the viability of BV2 cells. One thousand cells were added to each well of a 96-well plate, and the CCK-8 reagent was mixed with the medium at a ratio of 1:9 to form a working solution. 100 μL of working solution was added to each well and incubated for 1 h in a cell incubator. Cell viability was measured at 12 h after heme or paquinimod induction.

Flow cytometry

Flow cytometry was performed to assess neuronal death using an Annexin V PE/7-AAD kit (#CA1030, SolarBio, China). The data were analyzed using Novocyte Express (Santa Clara, CA, USA). The dead cell count was calculated using the following formula: [number of Annexin V PE+/7-AAD+ cells/number of total cells] × 100%.

Western Blot analysis

Brain tissue was weighed and lysed for protein extraction. Subsequently, the concentration of each sample was determined using the BCA method, followed by normalization. The extracted proteins were subjected to gel electrophoresis and the bands were transferred to a polyvinylidene difluoride (PVDF) membrane which was then washed and blocked in a 5% bovine serum albumin solution for 1 h. The membrane was then incubated with diluted primary antibody solution at 4°C overnight. The next day, the membrane was washed three times and

incubated with the appropriate secondary antibodies for 1 h at room temperature. Membrane bands were detected using an enhanced chemiluminescence (ECL) reagent kit (BL520B, Biosharp, China) after washing three times, and images were acquired using the ChemiDoc Touch Imaging System (BIORAD, USA). Images were analyzed using the ImageJ software (ImageJ 1.4, NIH, USA). The primary antibodies included anti-S100A9 (1:800, ab92507, Abcam, USA), anti-NLRP1 (1:1000, 12256-1-AP, Proteintech, USA), anti-iba1 (1:1000, ab283319, Abcam, USA), anti- TNF-α (1:1000, PAB36517, Bioswamp, China), anti-IL-1β (1:1000, PAB45925, Bioswamp, China), anti-IL-18 (1:1000, ab191860, Abcam, USA), anti-IL-6 (1:1000, 21865-1-AP, Proteintech, USA), anti- IκB-α (1:1000, 10268-1-AP, Proteintech, USA), anti-*p*-IκB-α (1:1000, 82349-1-RR, Proteintech, USA), anti-TLR4 (1:1000, PAB47910, Bioswamp, USA), anti-MYD88 (1:1000, PAB47936, Bioswamp, China), anti-NF-κB p65 (1:3000,80979-1-RR, Proteintech, USA), and anti-GAPDH (1:1000, GB15002, Servicebio, China). The secondary antibodies included HRP-labeled goat anti-rabbit (1:20,000; B0047, boerfu, China) and HRP-labeled goat anti-mouse (1:20,000; B0048, boerfu, China) antibodies.

QUANTIFICATION AND STATISTICAL ANALYSIS

Bioinformatic analysis was performed using R-studio (https://www.r-project.org/). Statistical analyses were conducted with GraphPad Prism 9.0 software (GraphPad Software, Inc.). Data from the experiments were presented as the mean ± SD. For data conforming to normality, we analyzed the significant differences among groups using the Student's *t* test. A nonparametric test or Kruskal–Wallis test was used to analyze the significant differences among groups in which the data failed to achieve normality. $p < 0.05$ was considered statistically significant.